Posterior Choroidal Stroma Reduces Accuracy of Automated Segmentation of Outer Choroidal Boundary in Swept Source Optical Coherence Tomography

Erandi Chandrasekera,[1–3] Evan N. Wong,[1,2] Danuta M. Sampson,[1,2] David Alonso-Caneiro,[1,4] and Fred K. Chen[1,2,5]

[1]Centre for Ophthalmology and Visual Science, The University of Western Australia, Perth, Australia
[2]Ocular Tissue Engineering Laboratory, Lions Eye Institute, Perth, Australia
[3]Save Sight Institute, The University of Sydney, Sydney, Australia
[4]Contact Lens and Visual Optics Laboratory, Queensland University of Technology, Brisbane, Australia
[5]Department of Ophthalmology, Royal Perth Hospital, Perth, Australia

PURPOSE. To determine the influence of choroidal boundary morphology on the accuracy of automated measurements of subfoveal choroidal thickness (SFCT) in swept source optical coherence tomography (SSOCT).

METHODS. A retrospective image analysis of foveal-centered horizontal line scans from normal and diseased eyes using the Topcon DRI OCT-1 Atlantis SSOCT was conducted. Subfoveal choroid-scleral junction (CSJ) and retina-choroidal junction (RCJ) morphologies were graded by two observers. Automated SFCT (A-SFCT) was compared with manual SFCT (M-SFCT) measurements from Bruch's membrane to the posterior limits of choroidal vessel, hyperreflective stroma, and hyporeflective lamina fusca. Agreement in boundary grading was assessed by Cohen's kappa. A-SFCT and M-SFCT were compared using Bland-Altman analysis and paired *t*-tests.

RESULTS. A total of 200 eyes of 100 patients with a mean (SD) age of 62 (18) years were included. The choroidal vessel, stromal, and lamina fusca boundaries were visible in 100%, 58%, and 38% of the eyes, respectively. Interobserver agreement in RCJ and CSJ grading was high (kappa = 0.974 and 0.851). Mean A-SFCT differed from M-SFCT by only 2 μm at posterior choroidal vessel boundary ($P = 0.801$). A-SFCT overestimated SFCT at the posterior vessel wall boundary by 17 μm ($P = 0.026$) and 23 μm ($P = 0.001$) in the presence of a visible posterior choroidal stroma and lamina fusca, respectively.

CONCLUSIONS. Automated outer choroidal boundary segmentation tends to identify the posterior limit of the choroidal vessel. Agreement between A-SFCT and M-SFCT is reduced by the presence of posterior stromal layer and lamina fusca. A-SFCT should be interpreted with RCJ and CSJ boundary grading.

Keywords: choroidal thickness, choroid-scleral boundary, suprachoroidal space, suprachoroidal layer, automated segmentation, manual segmentation, choroidal vessel, lamina fusca

Changes in choroidal thickness are implicated in the pathophysiology of various posterior segment pathologies.[1] Choroidal thickness has been shown to be important in the diagnosis and monitoring of diseases such as central serous chorioretinopathy (CSC), AMD, polypoidal choroidal vasculopathy, vitelliform pattern dystrophy, Vogt-Koyanagi-Harada syndrome, and choroidal tumors.[2,3] Accurate and reproducible measurements of choroidal thickness support the potential use of optical coherence tomography (OCT)-derived parameters for diagnosis, monitoring of disease progression and evaluating treatment response.[3,4]

Precise segmentation of the inner (the retina-choroid junction [RCJ]) and outer (choroid-scleral junction [CSJ]) boundaries of the choroid are essential for accurate choroidal thickness measurements.[4] The RCJ can be seen at the base of the outermost hyperreflective band representing the RPE/Bruch membrane (BM) complex in normal eyes and as a separate thin hyperreflective line when the RPE is detached (e.g., in pigment epithelial detachments or occult choroidal neovascularization) or absent (e.g., in geographic atrophy).[5] In contrast, the CSJ is not always clearly visible due to attenuation of signals by choroidal vessels and stroma, and regional variations in its appearance.[6] Swept source OCT (SSOCT) has enabled improved visualization of the CSJ and recent studies have reported that accurate choroidal thickness measurement is possible in 100% of eyes using an SSOCT device compared with 93% from spectral domain OCT (SDOCT) with enhanced depth imaging (EDI) technique.[7–9]

Previous studies have established good repeatability and reproducibility of automated choroidal thickness using an SSOCT instrument in healthy eyes[10-14]; however, there is now increased awareness of segmentation error in the demarcation of outer choroidal boundary in eyes with and without posterior segment pathology.[15] Furthermore, Yiu et al.[4] reported that

choroidal thickness measurements can vary up to 70 μm when taken to three different landmarks at the CSJ: vascular, stromal, and lamina boundaries. Accuracy of automated segmentation may be related to the variable appearance of the RCJ and CSJ, although data supporting this hypothesis are not available.[16]

Delineation of the inner and outer boundaries of the choroid by manual segmentation is time-consuming and, therefore, impractical for large number of B-scans in dense raster scan protocol used in clinical settings and large-scale population studies.[1,17,18] The different anatomic boundaries present at the CSJ may contribute to measurement variability between graders as demonstrated by several studies that reported moderate interobserver correlation coefficients of 0.6 to 0.8 using SSOCT.[5,6] Automated segmentation is available on the commercial software provided with the Topcon DRI OCT-1 Atlantis (Topcon Medical Systems, Paramus, NJ, USA) device to provide choroidal thickness profile along the B-scan; however, the accuracy of automated thickness and the exact location used as the posterior choroidal boundary by the software is unknown.

Herein, we examined the accuracy of automated choroidal thickness measurements provided by the Topcon DRI SSOCT device as compared with manual measurements in healthy and diseased eyes and explored its relationship with the type of RCJ and CSJ morphology at the subfoveal location.

METHODS

The study adhered to the tenets of the Declaration of Helsinki and was approved by the University of Western Australia Human Research Ethics Committee (RA/4/1/7227).

Study Participants

This is a cross-sectional consecutive retrospective chart and image review in a single institution, Lions Eye Institute, Perth, Western Australia. SSOCT images from subjects who had bilateral horizontal high-definition single line scans were exported from the database. Images were excluded from analysis if line scans were not taken through the foveal center or scan quality was reduced by shadow artifact from corneal opacity, dense cataract, or vitreous hemorrhage.

Variables and Data Collection

Age, sex, best corrected visual acuity (letter score from the Early Treatment of Diabetic Retinopathy Study chart) were recorded from the medical charts. All subjects included in the study had a retinal diagnosis for each eye made by the senior author (observer 1, FKC) based on clinical history, comprehensive examination, and multimodal imaging. RCJ and CSJ morphology on SSOCT scans were graded independently by observers 1 (FKC) and 2 (ENW). The main outcome variable was the difference between manual and automated subfoveal thickness measurements.

OCT Imaging Protocol

A single 30° 9.0-mm horizontal line scan averaging 96 frames, centered at the fovea, were taken of both eyes of each patient using the SSOCT device (Topcon DRI OCT-1 Atlantis). The device had an axial resolution of 8 μm and lateral resolution of 20 μm. The device automatically discarded image frames that could not be registered (due to fixation drift) so that in some patients, fewer than 96 frames were averaged for the final high-definition OCT image. The median (range) number of frames averaged for final high-definition OCT image was 76 (28–96). If

the preferred fixation locus was extrafoveal, the position of the line scan was moved manually until the foveal center was visualized at the center of the line scan before image acquisition.

Boundary Morphology Grading

Subfoveal choroidal thickness (SFCT) was defined as the perpendicular distance from the base of the RPE/BM complex or the BM (if RPE is elevated or absent) to one of the three various boundaries at the CSJ at the foveal center (i.e., RPE/BM is taken as the reference layer and used to calculate the normal to this surface).[19] It is, therefore, important to describe the different types of inner and outer choroidal boundaries in this cohort. Subfoveal RCJ was classified into three morphological types and graded using different letters (A, B, C). RCJ-A has normal single hyperreflective RPE/BM complex and the base of this serves as the inner choroid boundary (Fig. 1A). RCJ-B has a distinct thin hyperreflective line marking the BM as it has been separated from the broad hyperreflective band of the RPE due to a pigment epithelial detachment (PED) or choroidal neovascular (CNV) membrane (Fig. 1B). RCJ-C has a thickened or attenuated hyperreflective RPE/BM complex due to hyper-reflective subretinal lesions merging into the RPE band or loss of RPE/BM complex due to RPE atrophy (Fig. 1C). For final analysis, we kept the RCJ-C or RCJ-B grading instead of RCJ-A if there was discrepancy between the observers.

Subfoveal CSJ was also classified into three morphological types and graded using different numbers (CSJ-1, CSJ-2, CSJ-3). CSJ-1 is defined by the presence of large choroidal vessels as the only structure visible immediately anterior to the sclera (Fig. 1D). CSJ-2 was defined by the presence of an intervening distinct hyperreflective band of choroidal stroma separating the large choroidal vessels from the sclera (Fig. 1E). CSJ-3 was defined by the presence of an additional intervening hypore-flective lamina fusca (LF, also known as suprachoroidal space) separating the hyperreflective band of posterior choroidal stroma from the anterior scleral face (Fig. 1F). The grading of the boundaries applies only to the subfoveal location because segmentation error is examined only at this single location. For final analysis of the impact of boundary morphology on segmentation, the lower grading from the two observers was used if there was a discrepancy in boundary classification.

Manual Measurement

Manual SFCT (M-SFCT) measurement was taken from the BM to one or more boundaries present at the CSJ by two observers independently and averaged before comparison with automated SFCT (A-SFCT). There were potentially three measurements that could be made from the BM to the three interfaces of the CSJ depending on the type of CSJ. Eyes with CSJ-1 have one M-SFCT measurement (BM to the posterior choroidal vessel wall), those with CSJ-2 have two M-SFCT measurements (BM to posterior choroidal vessel wall and BM to the posterior edge of the choroidal stroma), and those with CSJ-3 have three M-SFCT measurements (BM to posterior choroidal vessel wall, BM to posterior edge of the choroidal stroma, and BM to the posterior edge of the LF) (Fig. 2).

Automated Measurement

The in-built software (version 9.00) on the Topcon SSOCT device was used to view automated segmentation and extract A-SFCT. Automated segmentation provided by the software demarcates "line 6" and "line 7," which corresponded to the RCJ and CSJ, respectively. The distance between these two lines at the foveal location was measured by observer 1 using
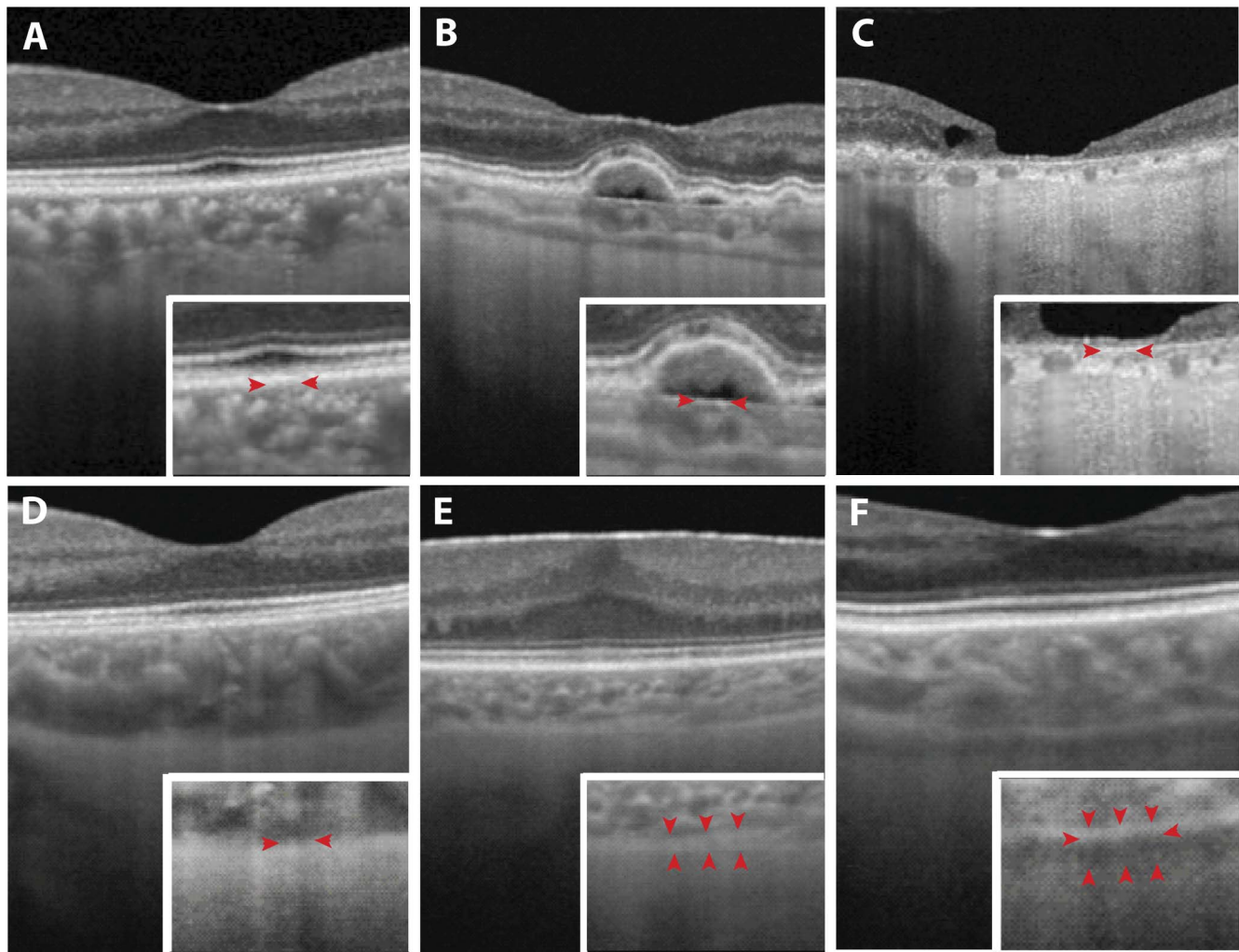
FIGURE 1. SSOCT images and magnified insets demonstrating the three types of RCJ: (A) RCJ-A, normal RPE/BM complex (*arrowheads*); (B) RCJ-B, thin hyperreflective line of BM (*arrowheads*) and a broad hyperreflective band of RPE separated from BM due to a PED; and (C) RCJ-C, RPE atrophy leaving a thin hyperreflective BM (*arrowheads*); and three types of CSJ: (D) CSJ-1, the presence of large choroidal vessels as the only structures visible immediately anterior to the sclera, the posterior choroidal vessel wall boundary is demarcated with *arrowheads*; (E) CSJ-2, presence of an intervening distinct hyperreflective band of choroidal stroma (demarcated with *arrowheads*) separating the large choroidal vessels from the sclera; and (F) CSJ-3, additional intervening hyporeflective band of LF (*arrowheads pointing upward*) separating the hyperreflective band of choroidal stroma (*arrowheads pointing downward*) from the anterior scleral face. The *horizontal arrowheads* show the boundary between the hyperreflective choroidal stroma and the hyporeflective LF.

the calipers in the onboard software and this value was recorded as the A-SFCT. Automated segmentation lines were not manually adjusted before observer 1 measuring the distance from line 6 to line 7. There was only one A-SFCT value per eye because the software did not seem to differentiate among the three types of CSJ. Error in automated segmentation of the BM and the posterior choroidal vessel boundary at the subfoveal location was recorded for each image. Frequency of error at RCJ, CSJ, or both RCJ and CSJ were tabulated for each combination of RCJ and CSJ morphology in a 3×3 format.

Statistical Analysis

Statistical analysis was carried out using SPSS Statistics for Windows Version 24.0 (IBM Corp., Armonk, NY, USA) and MedCalc for Windows, version 17.0 (MedCalc Software, Ostend, Belgium). Interobserver agreement between the two graders (observers 1 and 2) in classifying RCJ and CSJ of each eye was measured using Cohen's kappa test (κ). Kruskal-Wallis

H test and post hoc analysis (Dunn's test) was performed to explore the relationship between M-SFCT measured from the BM to the posterior choroidal vessel wall and CSJ morphology subtypes. Frequency of RCJ and CSJ segmentation error rates in those with RCJ-A versus RCJ-B and RCJ-C or CSJ-1 versus CSJ-2 and CSJ-3 were compared by using the χ^2 test. A P value of $<$ 0.05 was considered statistically significant.

Bland-Altman analysis was used to compare the single A-SFCT measurement with M-SFCT measurements taken from BM to each of the three CSJ boundaries (posterior choroidal vessel wall, posterior stromal boundary, posterior LF) in each image whenever visible. The mean difference and the 95% limit of agreement (LOA), defined as $\pm 1.96 \times$ SD, between A-SFCT and M-SFCT were shown in Bland-Altman plots. Significance of systematic bias between A-SFCT and M-SFCT was estimated using the paired-sample *t*-test and reported using mean and the SD of the difference. As exploratory analysis, the impact of RCJ and CSJ morphology on the difference between A-SFCT and M-SFCT measured to the posterior choroidal vessel wall was also examined.
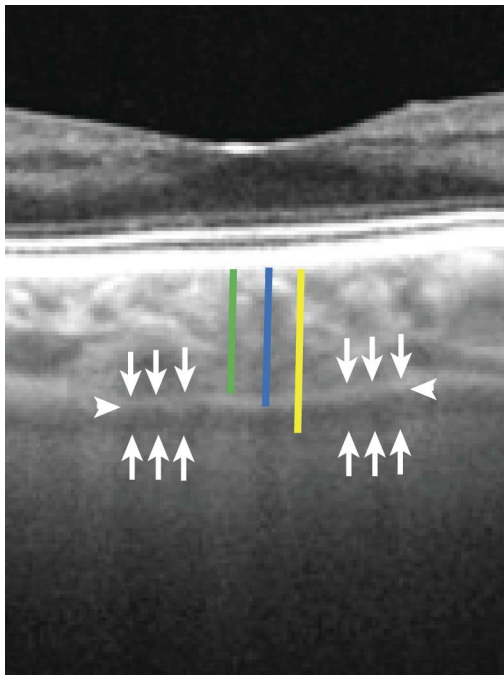
FIGURE 2. SSOCT image demonstrating CSJ-3 with three measurements: from BM to the posterior boundary of the choroidal vessel wall (*green*), posterior boundary of the hyperreflective choroidal stroma (*blue*), and posterior boundary of the hyporeflective lamina boundary (*yellow*). The hyperreflective band (*arrow pointing down*) of stroma is separated from hyporeflective band (*arrow pointing up*) of LF by a well-defined demarcation line (*horizontal arrows*). For illustrative purposes, the color lines have been separated. Measures in this study were taken below the foveal center.

RESULTS

Patient Demographics

A total of 200 eyes from 100 patients (51 men and 49 women) were included in our study. The mean (SD) age of the cohort was 62 (18) years (range, 13–89). Mean (SD) best corrected visual acuity score was 77 (12) letters (range, 14–97). Mean (SD) refractive error was −1.4 (0.6) Diopters. Frequency of each type of CSJ and RCJ boundary for each diagnostic category is shown in Table 1 and Supplementary Table S1, respectively.

Interobserver Agreement in RCJ and CSJ Classification

Both RCJ and CSJ were observed in all 200 eyes and graded by both observers. Both observers agreed that RCJ-A, RCJ-B, and RCJ-C were seen in 151 (75.5%), 42 (21%), and 5 (2.5%) eyes, respectively, at the subfoveal location ($\kappa = 0.974$, 95% confidence interval [CI] 0.937–1.000) (Supplementary Table S2). Both observers agreed that CSJ-1, CSJ-2, and CSJ-3 were seen in 74 (37%), 31 (15.5%), and 76 (38%) eyes, respectively, at the subfoveal location ($\kappa = 0.851$, 95% CI 0.787–0.915) (Supplementary Table S3).

Relationship Between choroidal thickness and CSJ Morphology Subtype

There was a statistically significant difference between M-SFCT at the posterior choroidal vessel wall between the different CSJ morphology types (CSJ-1, 2, 3), $\chi^2(2) = 13.401$, $P = 0.001$. The

TABLE 1. The Percentage of Eyes With CSJ-1, -2, and -3 in Each Category as Graded by Observers 1 and 2

Category	Category Description	*n*	CSJ-1, %	CSJ-2, %	CSJ-3, %
	All	200	42	20	38
1	Normal posterior segment	67	51	9	40
2	Diabetic retinopathy	7	57	14	29
3	AMD	83	28	26.5	45.5
	Drusen	42			
	Geographic atrophy	7			
	Neovascular AMD	34			
4	Myopic maculopathy	22	54.5	27.5	18
5	Other macular disease	21	52	24	24
	Vitreomacular traction and ERM	9			
	Retinal vein or artery occlusion	4			
	Choroidal folds	2			
	Choroidal nevus	2			
	Choroidal osteoma	1			
	Optic disc pit	1			
	Coats disease	1			
	Retinal dystrophy	1			

ERM, epiretinal membrane; *n*, number of eyes in each category as graded by observers 1 and 2 (in total agreement).

median thickness was 222.50 μm for CSJ-1, 160 μm for CSJ-2, and 182.75 μm for CSJ-3. Eyes with CSJ-1 were noted to have significantly thicker M-SFCT at the posterior choroidal vessel wall compared with eyes with CSJ-2 ($P = 0.002$) and CSJ-3 ($P = 0.032$) (Fig. 3). There was no statistically significant difference between CSJ-2 and CSJ-3 ($P = 0.591$).

Frequency of Segmentation Error as a Function of Boundary Morphology

The distribution of eyes with segmentation error in the RCJ, CSJ, or both are shown in Table 2. Among the 152 eyes with normal RCJ (type A, with no PED or RPE atrophy), only 12 had error at RCJ alone and 16 had error at both RCJ and CSJ with a combined frequency of 18% (28/152). However, among 48 eyes with abnormal RCJ (types B and C), 11 had error in RCJ
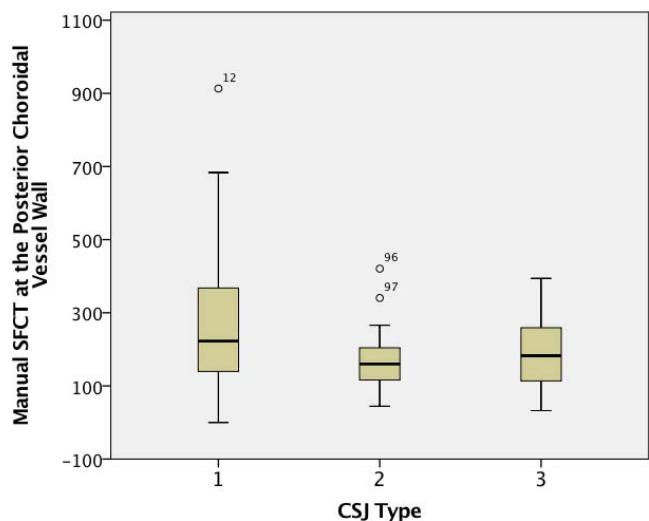

FIGURE 3. Boxplot demonstrating relationship between CSJ morphology type and manual SFCT at the posterior choroidal vessel wall.

TABLE 2. The Distribution of Eyes With Segmentation Error in the RCJ, CSJ, or Both

| | RCJ Type | | | | | | | | | | | |
| | A (*n* = 152) | | | | B (*n* = 42) | | | | C (*n* = 6) | | | |
Location of Segmentation Error	RCJ Only	CSJ Only	RCJ and CSJ	No Error	RCJ Only	CSJ Only	RCJ and CSJ	No Error	RCJ Only	CSJ Only	RCJ and CSJ	No Error
CSJ type												
1 (*n* = 84)	9	25	5	31	2	1	3	6	0	0	0	2
2 (*n* = 40)	0	9	5	11	3	3	4	3	0	1	1	0
3 (*n* = 76)	3	24	6	24	6	3	3	5	0	2	0	0
Total (*n* = 200)	12	58	16	66	11	7	10	14	0	3	1	2

alone and 11 had error at both RCJ and CSJ with a greater combined frequency of 46% (22/48). The difference in RCJ segmentation error rates was statistically significant ($\chi^2 = 14.6$, $P = 0.001$). Among the 84 eyes with classic CSJ morphology (type 1, only posterior vessel wall boundary present), 26 had error at CSJ and 8 had error at both RCJ and CSJ with a combined frequency of 40% (34/84). Similarly, 116 eyes with nonclassic CSJ morphology (types 2 and 3, with stromal and LF layers), 42 had error at CSJ and 19 had error at RCJ and CSJ with a combined frequency of 53% (61/116). Despite a trend for increased CSJ segmentation error rate in CSJ-2 and CSJ-3 subtypes, the difference was not statistically significant ($\chi^2 = 2.87$, $P = 0.091$).

Comparison Between A-SFCT and M-SFCT

All 200 eyes had a clearly visible posterior choroidal vessel wall, 116 of these also had a posterior choroidal stroma, and 76 also had a LF as graded by the observers 1 and 2 with complete agreement. The mean (SD) A-SFCT was 218 (101) μm. The mean (SD) M-SFCT were 216 (132), 230 (102), and 270 (109) μm measured to the posterior limits of choroidal vessel, choroidal stroma, and the LF, respectively. The differences between A-SFCT and M-SFCT at each of the three boundaries were not normally distributed (Shapiro-Wilk $P < 0.005$). However, there was a strong central tendency toward the mean. A-SFCT overestimated SFCT by a mean (SD) of 2 (100) μm ($P = 0.801$), and underestimated SFCT by a mean (SD) of 26 (66) μm ($P < 0.0001$) and 54 (75) μm ($P < 0.0001$) at the three posterior boundaries, respectively (Table 3; Fig. 4). Although there was a tendency for automated segmentation to underestimate posterior vessel wall boundary in thicker choroids (Fig. 4A), there was no overall relationship between difference and mean thickness.

Predictors of Agreement Between A-SFCT and M-SFCT

Impact of RCJ Morphology on Difference Between A-SFCT and M-SFCT. There were no significant differences between A-SFCT and M-SFCT to the posterior choroidal vessel wall in eyes with RCJ-A ($P = 0.380$) and RCJ-C ($P = 0.254$) morphology, respectively. Eyes with RCJ-B had a statistically significantly higher mean difference of 20 μm ($P = 0.002$) compared with M-SFCT (Figs. 5A–C; Table 4).

Impact of Choroid-Sclera Junction Morphology on A-SFCT and M-SFCT. A-SFCT measurement underestimated SFCT at the posterior choroidal wall by 25 μm ($P = 0.100$) in eyes with CSJ-1. In contrast, A-SFCT overestimated SFCT by 17 μm ($P = 0.026$) and 23 μm ($P = 0.001$) in CSJ-2 and CSJ-3, respectively (Table 5). A-SFCT measurement underestimated SFCT at the stromal boundary by 28 μm ($P = 0.004$) in CSJ-2 eyes and 25 μm ($P = 0.003$) in eyes with CSJ-3. A-SFCT

measurement also underestimated SFCT at the posterior lamina boundary by 54 μm ($P < 0.001$) in CSJ-3 eyes (Table 5; Figs. 5D–F).

DISCUSSION

This is the first study to demonstrate the influence of boundary morphology on systematic error in A-SFCT measurements using SSOCT. Although A-SFCT was similar to M-SFCT when measured to the posterior choroidal vessel wall, there were significant differences when A-SFCT was compared with M-SFCT measured to posterior stromal and LF boundaries. The largest discrepancy between A-SFCT and M-SFCT (to choroidal vessel wall) was seen in eyes with RCJ-B (PED, CNV) and in eyes with a choroidal stroma (CSJ-2) and a LF (CSJ-3).

Although there were differences in proportions of RCJ and CSJ boundary types across different disease groups, there was good interobserver agreement in grading of these boundaries. Although two other studies have discussed grading of outer choroidal boundary morphology and reported the frequencies of different types of CSJ boundaries in eyes with different posterior segment pathology, neither have confirmed interobserver agreement with statistical analysis.[4,20] CSJ-3 (eyes with a choroidal stroma and LF) was the second most prevalent CSJ type and was found in 40% of 67 healthy eyes in our cohort (mean age 62). This was similar to the findings by Yiu et al.,[4] who analyzed 74 healthy eyes (mean age 68.6 years) using EDI SDOCT and found that 44.6% had a visible LF. They noted that visibility of the LF was associated with a hyperopic refractive error. Conversely, we also visualized LF less frequently in pathologic myopia (18%) compared with the normal eyes (40%). Michalewska et al.[20] also reported that the suprachoroidal layer, SCL (hyperreflective stromal band ± a hyporeflective SCS) was rarely visualized in myopic or emmetropic eyes. In contrast, our study found that the choroidal stroma and LF were visible in 27.5% and 18.0% of the pathologic myopia group, respectively. The difference may be related to

TABLE 3. Difference Between A-SFCT and M-SFCT Measured to Three Different Posterior Choroidal Boundaries

A-SFCT − M-SFCT	*n*	Mean, μm	Min, μm	Max, μm	SD, μm	P, Paired Samples *t*-Test
Posterior vessel wall boundary	200	+2	−643	+326	100	0.801
Posterior stromal boundary	116	−26	−216	+196	66	<0.0001
Posterior LF boundary	76	−54	−251	+178	75	<0.0001

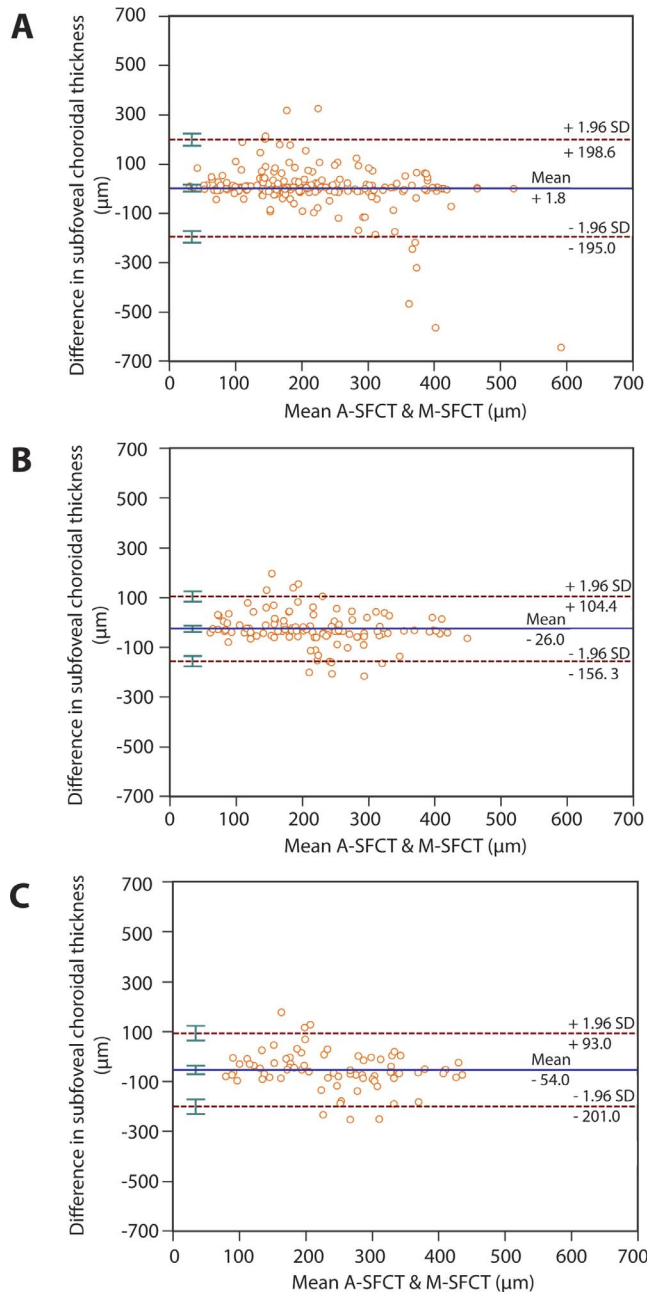Max, maximum; Min, minimum; *n*, number of eyes in each category as graded by observer 1.

FIGURE 4. Bland-Altman plots of the difference in SFCT between A-SFCT and M-SFCT measurements plotted against the mean of A-SFCT and M-SFCT measured to (**A**) the posterior choroidal vessel wall boundary ($n = 200$); 95% CI for mean: -12 to 16 μm, 95% CI for lower LOA: -219 to -171 μm, 95% CI for upper LOA: 175 to 222 μm; (**B**) the posterior choroidal stroma boundary ($n = 116$); 95% CI for mean: -38 to 14 μm, 95% CI for lower LOA: -177 to -135 μm, 95% CI for upper LOA: 83 to 125 μm; and (**C**) the posterior LF boundary ($n = 76$); 95% CI for mean: -71 to -38 μm, 95% CI for lower LOA: -230 to -172 μm, and 95% CI for upper LOA: 64 to 122 μm. The *solid horizontal line* is the mean bias and the *two dotted lines* are the LOA defined by mean ± $1.96 \times$ SD.

the inclusion of myopic eyes with foveoschisis, staphyloma, and choroidal neovascularization in our myopia group.

We found a relationship between increased subfoveal choroid thickness and CSJ-1 morphology subtype at the fovea. Although this relationship may not hold true for boundary morphology across all locations in the submacular region, we

TABLE 4. Relationship Between RCJ Morphology and Difference Between M-SFCT and A-SFCT Measured to the Posterior Vessel Wall Boundary

A-SFCT − M-SFCT	n	Mean, μm	Min, μm	Max, μm	SD, μm	P, Paired Samples t-Test
RCJ-A	152	-7.7	-643	$+325$	108	0.380
RCJ-B	42	$+20$	-168	$+154$	59	0.002
RCJ-C	6	$+47$	-49	$+214$	89	0.254

Max, maximum; Min, minimum; n, number of eyes in each category as graded by Observer 1.

offer two explanations for this observation. First, reduced OCT signal penetration through a thicker choroid led to a loss of visibility of the posterior stromal layer and LF. Second, choroidal vessel permeability is increased in eyes with thicker choroid. Increased choroidal thickness has been associated with diseases such as central serous chorioretinopathy in which hyperpermeability of the choroidal vessels is thought to play an important role. Increased choroidal venous pressure is associated with choroidal detachment (fluid in the LF space) in the peripheral fundus as seen in uveal effusion syndrome. However, this phenomenon is not encountered clinically in the macular region, perhaps due to the numerous short posterior ciliary arteries tethering the uveal tissue to the sclera preventing fluid accumulation in LF. Instead, submacular choroidal vessel hyperpermeability may lead to increased interstitial fluid compressing the posterior stromal layer and obliterate the LF layer resulting in CSJ-1 morphology rather than CSJ-2 or CSJ-3. More detailed study of the variability in CSJ morphology across the entire submacular region and longitudinal studies in patients with central serous chorioretinopathy treated with photodynamic therapy may provide more insight into the relationship between choroidal venous pressure, permeability, and CSJ morphology.

Our study found a small nonsignificant mean difference of 2 μm between A-SFCT and M-SFCT measured to the posterior vessel wall boundary. However, there was a trend toward underestimation of the subfoveal choroidal thickness at the posterior vessel wall boundary due to error in automated segmentation in eyes with thicker choroid (Fig. 4A). Michalewski et al.[21] reported that automated thickness measurement

TABLE 5. Relationship Between CSJ Morphology and Difference Between M-SFCT and A-SFCT Measured to Three Different Posterior Choroidal Boundaries

A-SFCT − M-SFCT	n	Mean, μm	Min, μm	Max, μm	SD, μm	P, Paired Samples t-Test
CSJ-1	84					
Posterior vessel wall		-25	-643	$+325$	138	0.100
CSJ-2	40					
Posterior vessel wall		$+17$	-49	$+154$	47	0.026
Posterior stromal boundary		-28	-158	$+130$	56	0.004
CSJ-3	76					
Posterior vessel wall		$+23$	-115	$+214$	59	0.001
Posterior stromal boundary		-25	-216	$+196$	53	0.003
Posterior lamina boundary		-54	-251	$+178$	75	<0.001

Max, maximum; Min, minimum; n, number of eyes in each category as graded by observer 1.
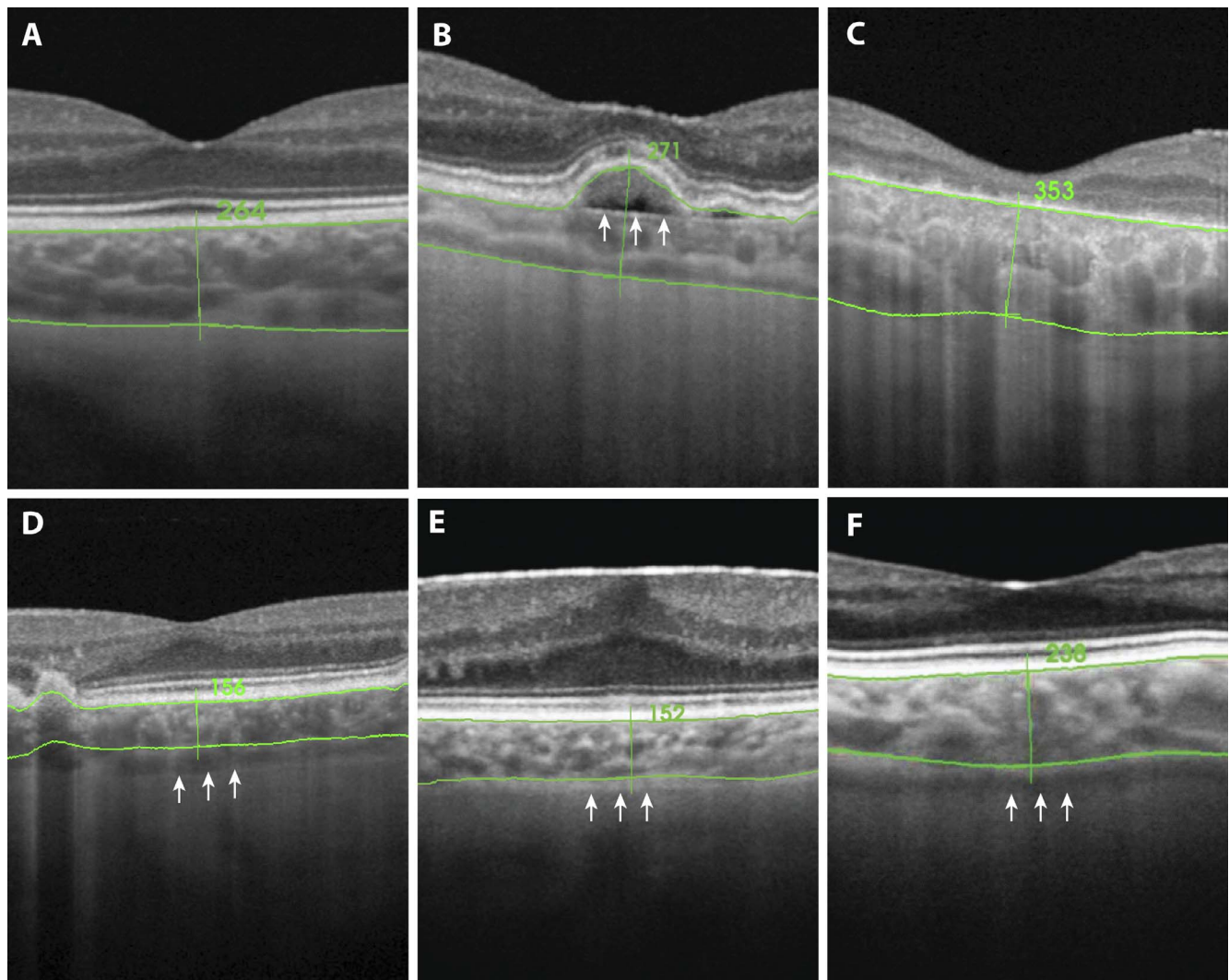
FIGURE 5. SSOCT images at the level of the fovea with automatic segmentation lines (*green*) demonstrating examples of the most common errors seen in our study in RCJ-A, -B, and -C, and CSJ-1, -2, and -3, respectively. (**A**) RCJ-A with a normal RPE/BM complex with correct demarcation (*horizontal green line* at the superior aspect of image). (**B**) RCJ-B with a pigment epithelial defect where the automated segmentation has incorrectly detected the RPE (*horizontal green line* at the superior aspect of image) instead of BM (*arrows*). (**C**) RCJ-C with RPE atrophy and a faint hyperreflective BM that has been correctly segmented (*horizontal green line* at the superior aspect of image). (**D**) CSJ-1 where the automated segmentation (*horizontal green line* at the inferior aspect of the image) has incorrectly underestimated the posterior choroidal vessel wall (*arrows*). (**E**) CSJ-2 where the automated segmentation (*horizontal green line* at the inferior aspect of the image) has incorrectly detected the posterior choroidal vessel wall instead of the posterior border of the hyperreflective choroidal stroma (*arrows*). (**F**) CSJ-3 where the automated segmentation (*horizontal green line* at the inferior aspect of the image) has detected the posterior choroidal vessel border instead of the posterior border of the hyporeflective LF (*arrows*).

underestimated manual thickness by 38 µm in healthy individuals; however, they manually measured to the posterior stromal or LF boundary, whichever formed the outermost limit of the CSJ rather than the use of a consistent definition such as the posterior vessel wall boundary.[21] Zafar et al.[22] also reported relatively high discrepancies between automated and manual thickness measurements of 33 µm in normal and 42 µm in diseased eyes, but they did not specify the anatomic location they measured to at the CSJ. In contrast, other studies using normal eyes found relatively small mean differences of <1 µm (Philip et al.[23]), <15 µm (Zhang et al.[24]), and 12.96 µm in paediatric eyes and 16.27 µm in adult eyes (Alonso-Caneiro et al.[25]). However, none of these studies defined which of the three anatomic boundaries were used as the CSJ when acquiring manual measurements.

In this study, we also investigated the influence of RCJ and CSJ morphology on the disagreement between A-SFCT and M-SFCT. Although the differences between A-SFCT and M-SFCT were not significant in eyes with normal RPE/BM (mean −7.7 µm, $P = 0.380$) (Fig. 5A) or atrophic RPE (mean 47 µm, $P = 0.254$) (Fig. 5C), automated segmentation significantly overestimated M-SFCT when there was pathology causing separation of BM from the RPE, such as PED, CNV (mean 26 µm, $P = 0.002$) (Fig. 5B). In these eyes, it was noted that the segmentation algorithm mistakenly marked the RPE as the RCJ rather than BM. We postulated that this was due to the increased hyperreflectivity of the RPE compared with BM when these two structures were separated by CNV or in PED. This observation was also supported by the higher frequency of automated RCJ segmentation error (46%) in eyes with RCJ-B and RCJ-C compared with the normal RCJ-A subtype (18%). Although automated methods were somewhat accurate in identifying the posterior choroidal vessel wall limit, true SFCT could not be measured in eyes with CSJ-2 and CSJ-3 due to the

complexity of reflectivity profile introduced by the hyper-reflective stroma and hyporeflective LF. Even in the simplest form of CSJ (CSJ-1) there was a bias (not statistically significant) toward underestimation of SFCT (25 μm) by automated segmentation with excessively large range of differences of up to 970 μm. In contrast, automated segmentation tends to identify the outer choroidal boundary somewhere within the hyperreflective stroma, resulting in a systematic error of overestimation of the SFCT (by 17 and 23 μm) measured to the posterior choroidal vessel wall among eyes with more complex CSJ (CSJ-2 and CSJ-3). We found a trend for increased CSJ segmentation error (53% versus 40%) in eyes with posterior stromal or LF layers (i.e., CSJ-2 and CSJ-3) compared with those without (CSJ-1). However, the difference between automated and manual choroidal thickness measurement at the posterior stromal boundary and LF did not vary with increasing thickness of the choroid (Figs. 4B, 4C). The studies by Hu et al.[26] and Kong et al.[15] were the only two studies to assess automated segmentation error rates at both RCJ and CSJ in healthy and diseased eyes. However, neither study investigated the effects of different RCJ and CSJ morphology on the accuracy of automated segmentation. Furthermore, they measured choroidal thickness to only one anatomic location at the CSJ.[15] Hu et al.[26] found the mean (SD) difference between algorithm and manual segmentation of boundary location was −0.74 (3.27) μm for the RCJ and −3.9 (15.93) μm for the CSJ. However, they used only 30 eyes, with only 10 diseased eyes with one type of pathology (non-neovascular AMD).[26] Kong et al.[15] studied 89 pathological eyes and normal fellow eyes and reported an error rate in automated choroidal segmentation at the RCJ ranging from 0% in normal eyes to 24% in eyes with retinochoroidal pathology. At the CSJ, a much higher segmentation error rate, ranging from 6% in normal eyes to 68% in eyes with retinochoroidal pathology, was noted.[15] Similar to our study, they also reported higher segmentation error rates at the CSJ in comparison with the RCJ. The highest error rates at both boundaries were found in eyes with chorioretinal pathology in comparison with normal eyes or eyes with purely retinal pathology.

There are several limitations in the present study. First, we only analyzed measurement at the subfoveal location rather than choroidal thickness profile along the entire length of the B-scan. Furthermore, only one B-scan per eye was analyzed. The complexity of boundary grading would increase significantly if the entire length of the B-scan or a raster set was graded due to the variation in CSJ and RCJ morphology across the macular region. Second, we included a wide range of pathology including both eyes of each patient and, therefore, our result cannot be applied to any specific disease or patient cohort. Third, we investigated the accuracy of automated segmentation when it was applied to a single B-scan rather than a series of raster scans. The accuracy of automated segmentation may be improved when multiple scans are segmented concurrently.

Although there are differences in proportions of RCJ and CSJ morphology types across different posterior segment pathology, we found good interobserver agreement in choroidal boundary grading. Although the overall mean difference between automated and manual SFCT measurements to the posterior vessel wall was only 2 μm, the discrepancy can be much larger. The disagreement in SFCT was increased in eyes with RCJ-B (PED, CNV) and in CSJ-2 and CSJ-3. We caution the use of SFCT measurements derived from automated algorithms without RCJ and CSJ grading or manual correction of segmentation errors. Deep learning neural network may be necessary to classify and identify variations in the inner and outer choroidal boundaries in healthy and diseased eyes to improve automated segmentation of the choroid.

References

1. Lu H, Boonarpha N, Kwong MT, Zheng Y. Automated segmentation of the choroid in retinal optical coherence tomography images. *Conf Proc IEEE Eng Med Biol Soc*. 2013; 2013:5869–5872.

2. Ruiz-Medrano J, Flores-Moreno I, Pena-Garcia P, Montero JA, Duker JS, Ruiz-Moreno JM. Macular choroidal thickness profile in a healthy population measured by swept-source optical coherence tomography. *Invest Ophthalmol Vis Sci*. 2014;55: 3532–3542.

3. Moisseiev E, Loewenstein A, Yiu G. The suprachoroidal space: from potential space to a space with potential. *Clin Ophthalmol*. 2016;10:173–178.

4. Yiu G, Pecen P, Sarin N, et al. Characterization of the choroid-scleral junction and suprachoroidal layer in healthy individuals on enhanced-depth imaging optical coherence tomography. *JAMA Ophthalmol*. 2014;132:174–181.

5. Ikuno Y, Maruko I, Yasuno Y, et al. Reproducibility of retinal and choroidal thickness measurements in enhanced depth imaging and high-penetration optical coherence tomography. *Invest Ophthalmol Vis Sci*. 2011;52:5536–5540.

6. Tian J, Marziliano P, Baskaran M, Tun TA, Aung T. Automatic segmentation of the choroid in enhanced depth imaging optical coherence tomography images. *Biomed Opt Express*. 2013;4:397–411.

7. Wei WB, Xu L, Jonas JB, et al. Subfoveal choroidal thickness: the Beijing Eye Study. *Ophthalmology*. 2013;120:175–180.

8. Copete S, Flores-Moreno I, Montero JA, Duker JS, Ruiz-Moreno JM. Direct comparison of spectral-domain and swept-source OCT in the measurement of choroidal thickness in normal eyes. *Br J Ophthalmol*. 2014;98:334–338.

9. Ruiz-Medrano J, Flores-Moreno I, Montero JA, Duker JS, Ruiz-Moreno JM. Morphologic features of the choroidoscleral interface in a healthy population using swept-source optical coherence tomography. *Am J Ophthalmol*. 2015;160:596–601.

10. Adhi M, Ferrara D, Mullins RF, et al. Characterization of choroidal layers in normal aging eyes using enface swept-source optical coherence tomography. *PLoS One*. 2015;10: e0133080.

11. Han YS, Lim HB, Lee SH, Kim JY. Diurnal variation in choroidal and retinal thickness of the early treatment of diabetic retinopathy study macular subfields determined using swept-source optical coherence tomography. *Ophthalmologica*. 2015;233:192–197.

12. Nagasawa T, Mitamura Y, Karome T, et al. Macular choroidal thickness and volume in healthy pediatric individuals measured by swept-source optical coherence tomography. *Invest Ophthalmol Vis Sci*. 2013;54:7068–7074.

13. Mansouri K, Medeiros FA, Marchase N, Tatham AJ, Auerbach D, Weinreb RN. Assessment of choroidal thickness and volume during the water drinking test by swept-source optical coherence tomography. *Ophthalmology*. 2013;120: 2508–2516.

14. Park HY, Shin HY, Park CK. Imaging the posterior segment of the eye using swept-source optical coherence tomography in myopic glaucoma eyes: comparison with enhanced-depth imaging. *Am J Ophthalmol*. 2014;157:550–557.

15. Kong M, Eo DR, Han G, Park SY, Ham DI. Error rate of automated choroidal segmentation using swept-source optical coherence tomography. *Acta Ophthalmol*. 2016;94:e427–e431.

16. Huynh E, Chandrasekera E, Bukowska D, McLenachan S, Mackey DA, Chen FK. Past, present, and future concepts of the choroidal scleral interface morphology on optical coherence tomography. *Asia Pac J Ophthalmol (Phila)*. 2017;6:94–103.

17. Mansouri K, Medeiros FA, Tatham AJ, Marchase N, Weinreb RN. Evaluation of retinal and choroidal thickness by swept-source optical coherence tomography: repeatability and assessment of artifacts. *Am J Ophthalmol*. 2014;157:1022–1032.

18. Chiu SJ, Li XT, Nicholas P, Toth CA, Izatt JA, Farsiu S. Automatic segmentation of seven retinal layers in SDOCT images congruent with expert manual segmentation. *Opt Express*. 2010;18:19413–19428.

19. Alonso-Caneiro D, Read SA, Vincent SJ, Collins MJ, Wojtkowski M. Tissue thickness calculation in ocular optical coherence tomography. *Biomed Opt Express*. 2016;7:629–645.

20. Michalewska Z, Michalewski J, Nawrocka Z, Dulczewska-Cichecka K, Nawrocki J. Suprachoroidal layer and suprachoroidal space delineating the outer margin of the choroid in swept-source optical coherence tomography. *Retina*. 2015;35:244–249.

21. Michalewski J, Michalewska Z, Nawrocka Z, Bednarski M, Nawrocki J. Correlation of choroidal thickness and volume measurements with axial length and age using swept source optical coherence tomography and optical low-coherence reflectometry. *Biomed Res Int*. 2014;2014:639160.

22. Zafar S, Siddiqui MR, Shahzad R. Comparison of choroidal thickness measurements between spectral-domain OCT and swept-source OCT in normal and diseased eyes. *Clin Ophthalmol*. 2016;10:2271–2276.

23. Philip AM, Gerendas BS, Zhang L, et al. Choroidal thickness maps from spectral domain and swept source optical coherence tomography: algorithmic versus ground truth annotation. *Br J Ophthalmol*. 2016;100:1372–1376.

24. Zhang L, Buitendijk GHS, Lee K, et al. Validity of automated choroidal segmentation in SS-OCT and SD-OCT. *Invest Ophthalmol Vis Sci*. 2015;56:3202–3211.

25. Alonso-Caneiro D, Read SA, Collins MJ. Automatic segmentation of choroidal thickness in optical coherence tomography. *Biomed Opt Express*. 2013;4:2795–2812.

26. Hu Z, Wu X, Ouyang Y, Ouyang Y, Sadda SR. Semiautomated segmentation of the choroid in spectral-domain optical coherence tomography volume scans. *Invest Ophthalmol Vis Sci*. 2013;54:1722–1729.